NURETH14-385

GEOMETRIC EFFECTS OF 90-DEGREE VERTICAL ELBOWS ON LOCAL TWO-PHASE FLOW PARAMETERS

M. Yadav, T. Worosz and S. Kim The Pennsylvania State University, University Park, PA, USA

Abstract

This study presents the geometric effects of 90-degree vertical elbows on the development of the local two-phase flow parameters. A multi-sensor conductivity probe is used to measure local two-phase flow parameters. It is found that immediately downstream of the vertical-upward elbow, the bubbles have a bimodal distribution along the horizontal radius of the pipe cross-section causing a dual-peak in the profiles of local void fraction and local interfacial area concentration. Immediately downstream of the vertical-downward elbow it is observed that the bubbles tend to migrate towards the inside of the elbow's curvature. The axial transport of void fraction and interfacial area concentration indicates that the elbows promote bubble disintegration. Preliminary predictions are obtained from group-one interfacial area transport equation (IATE) model for vertical-upward and vertical-downward two-phase flow.

Introduction

In a thermal-hydraulic system, coolant flows through channels of different sizes and orientations that are interconnected via various junctions and flow restrictions. During normal operating conditions and under postulated reactor accident conditions, two-phase flow exists where changes in the interfacial structures govern the transport phenomena. However, there is a lack of experimental data and knowledge of the mechanisms that govern the development of the twophase structures through flow restrictions. Such limitations present shortcomings in the thermalhydraulic analysis of nuclear reactor systems. Since the mass, momentum and energy transfer of any two-phase flow are greatly influenced by the interfacial structures and their transport characteristics, experimental studies are crucial in improving the understanding of the effects of flow restrictions on two-phase flow parameters and development of dynamic models for interfacial area. A number of studies in past have been performed in either vertical sections alone or horizontal sections alone. Among the limited studies on effect of flow restrictions on interfacial structures, Kim et al [1] and Talley et al [2] investigated the geometric effects of a 90degree and 45-degree elbow respectively, in horizontal bubbly flow. Yadav et. al [3] compared the geometric effects of 90-degree and 45-degree elbow in horizontal two-phase flow and demonstrated characteristic similarities and differences in the elbow-effects. Current study addresses the major effects of 90-degree vertical elbows connecting vertical-to-horizontal-tovertical sections on the local interfacial structures such as: void fraction, interfacial area concentration, bubble velocity and bubble size.

1. Experimental facility and test conditions

The experiments are performed at room temperature, 25 °C, and atmospheric pressure. The experimental facility consists of vertical-horizontal test sections made out of 50.8 mm inner diameter acrylic pipes connected by 90-degree vertical glass elbows. A schematic of the test facility is shown in Figure 1. The lengths of vertical and horizontal sections are 3.35m and 9.45m, yielding development lengths of 66 and 186 diameters, respectively. Along the test section 24 measurement locations with a total of 15 moveable measurement ports are available as shown in Figure 1. These measurement ports are designed to facilitate pressure measurement, local conductivity probe measurements, optical measurements, and flow visualization. A detailed description of the test facility can be obtained from [4]. A total of six flow conditions, as shown in Table 1, are chosen to obtain local two-phase flow parameters. The flow conditions are selected to be within or near the bubbly flow regime in the vertical-upward section and horizontal section based on the modified flow regime maps for the facility [4].

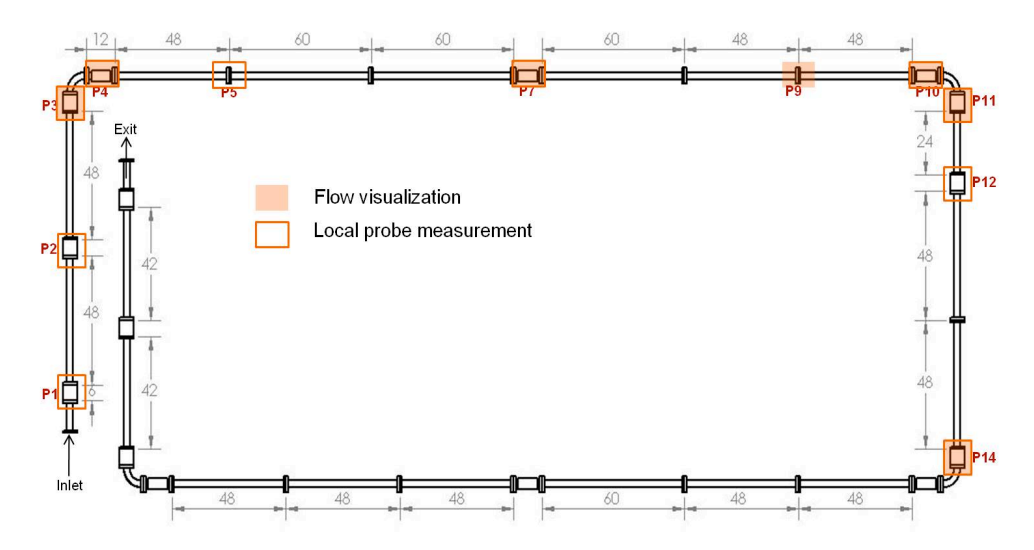


Figure 1 Simplified schematic of the combinatorial two-phase flow facility.

TC 11 1	C. 1.CC	1 1 1 1 1 1 1 1 1 1 1 1 1 1 1 1 1 1 1 1	1, 1, 1	1, 1 (١
Table I	Niv different to	act conditions lie	ed to obtain loca	l two_nhace t	low narameters
I ainc i	DIA UITICICIIL II	cat containona ua	cu w omani wca	i two-bhase i	iow parameters

Run No.	Run1	Run2	Run3	Run4	Run5	Run6
j _{g,atm} [m/s]	0.14	0.23	0.34	0.14	0.23	0.35
$j_f[m/s]$	2.0	2.0	2.0	3.0	3.0	3.0

2. Results and discussion

A four-sensor conductivity probe [5] is used to measure local two-phase flow parameters along the test section. The measured parameters include void fraction, bubble velocity, interfacial area concentration (a_i) and bubble frequency. Local two-phase flow parameters are measured at ten different axial locations along the test section. Accordingly, the analysis is divided into measurements in the vertical-upward section, horizontal section (downstream of the vertical-upward elbow), and vertical-downward section (downstream of the vertical-downward elbow).

The statistical error associated with the measurement using a double-sensor conductivity probe is approximately $\pm 7\%$. The error may arise from various factors such as bubble lateral motion, bubble velocity fluctuations, probe spacing and intrusiveness of the probe. A detailed analysis on the errors due to the probe can be found in the study by Wu and Ishii [6]. To benchmark the probe measurements, superficial gas velocity at each port determined from the probe measurements ($<\alpha v_g>_{loc}$) is compared with $< j_g>_{loc}$ based on gas flow and pressure measurements. The results, shown in Figure 2, indicate relatively good agreement within $\pm 10\%$ difference. It should be noted that the above benchmarking is only accurate for bubbly flows. Since, many of the bubbly flow conditions in the vertical-upward section transition to plug or slug flow in the horizontal section and vertical-downward section, the error in the pressure measurement increases significantly which reduces the reliability of $< j_g>_{loc}$ as a benchmark. This occurs for Runs 1, 2, and 3 at port P11 which correspond to the highest deviations shown in the figure.

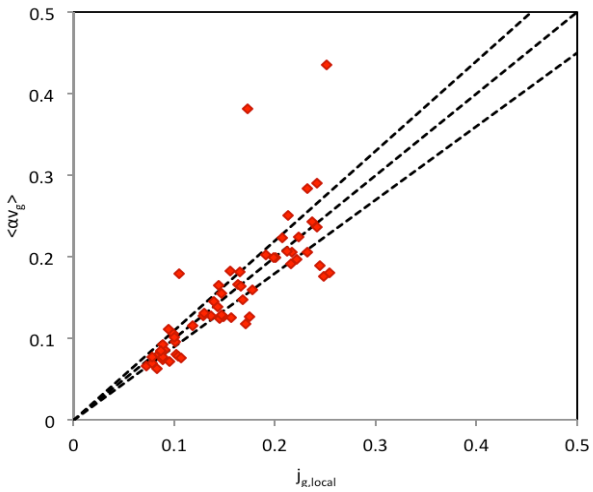


Figure 2 Comparison of local superficial gas velocity, $\langle j_g \rangle_{loc}$ measured by flow meter with $\langle \alpha v_g \rangle$ acquired by the conductivity probe; dotted lines represent $\pm 10\%$ deviation.

2.1 Interfacial structures in the vertical-upward section

In the vertical-upward section, local measurements are obtained at ports P1, P2, and P3, which are located at 6D, 33D, and 54D downstream of the inlet. The bubble distribution in the vertical-upward section is found to be axisymmetric, and hence, local measurements are only obtained along a half-diameter of the pipe cross-section. Figure 3 shows the development of the local void fraction and a_i profiles along the vertical section for Run 4. The local void fraction is indicative of the gas-phase distribution across the pipe cross-section. It is found that for all the flow conditions investigated the bubble distribution changes from center-peaked at port P1 to wall-peaked as it progresses along the vertical section. The degree of wall-peak depends upon the axial location as well as the gas flow rate. At port P1, the inlet effects dictate the bubble distribution. The bubble distribution in the developed two-phase flow is governed by various hydrodynamic forces and wall effects [7], which lead to a wall-peak. Since, the measurements are made under bubbly flow conditions the a_i profiles are similar to the void fraction profiles.

The effect of gas flow rate on interfacial structures in the vertical-upward section is shown in Figure 4. Here, the profiles of local void fraction and a_i at different axial locations are shown for a constant liquid flow rate, $j_f = 3.0$ m/s and increasing gas flow rates. In general, the local void

fraction increases with increasing gas flow rate. Moreover, increasing the gas flow rate also affects the axial development of the bubble distribution across the pipe cross-section. As is evident from the figure, the local void fraction profiles are center peaked at port P1 for all of the flow conditions. Similarly, all of the local void fraction profiles are wall peaked at port P2. However, at port P3 the bubble distribution changes with increasing gas flow rate. It is found that the void fraction profile changes from wall- peaked to center-peaked as the gas flow rate increases.

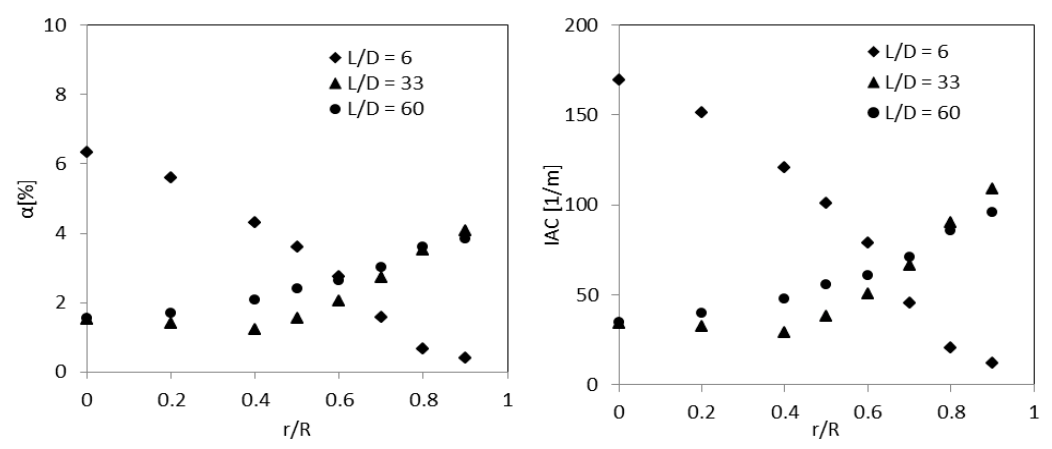
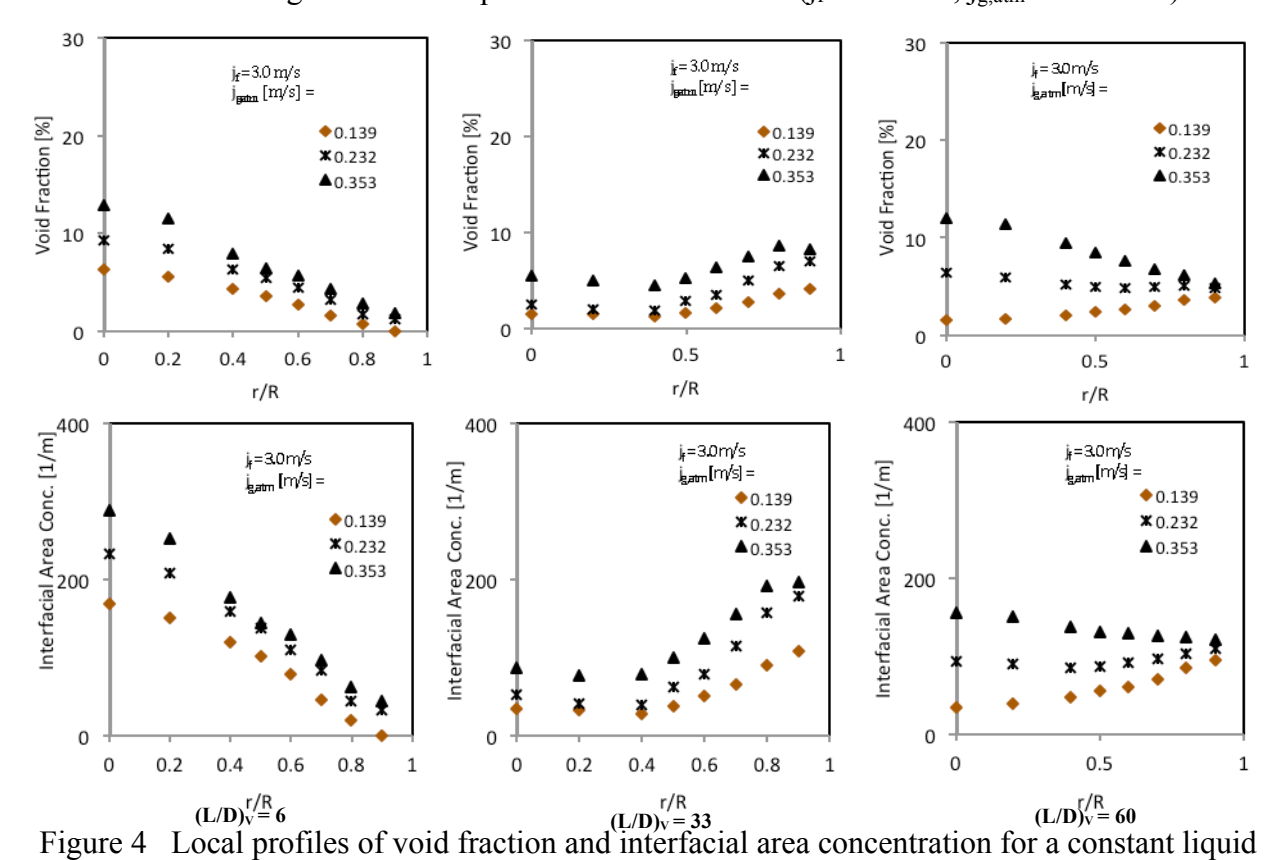


Figure 3 Local profiles of void fraction and interfacial area concentration at different axial locations along the vertical-upward section for Run 4 ($j_f = 3.0 \text{ m/s}$, $j_{g,atm} = 0.14 \text{ m/s}$).



flow rate, $j_f = 3.0$ m/s and increasing gas flow rates, along the vertical-upward section.

2.2 Interfacial structures in the horizontal section

Local two-phase flow parameters in the horizontal section are measured at four measurement ports P4, P5, P7 and P10, which are located at development lengths of 3D, 30D, 90D, and 170D downstream of the vertical-upward elbow. The bubble distribution in the horizontal section is asymmetric due to the buoyancy and elbow effects. Hence, local measurements are obtained across the entire pipe cross-section. The horizontal measurement port, shown in Figure 5a, is designed such that it can be rotated at 22.5° intervals in the azimuthal direction. The measurement scheme used in the horizontal section is shown in Figure 5b. Here, r/R_V and r/R_H denote the vertical and horizontal axes of the pipe cross-section, respectively. The direction of flow is into the plane. At each of the eight angular positions, the conductivity probe is traversed to fifteen different radial positions. Hence, at a given axial location for a given flow condition a total of 120 local data points are measured across the entire pipe cross-section.

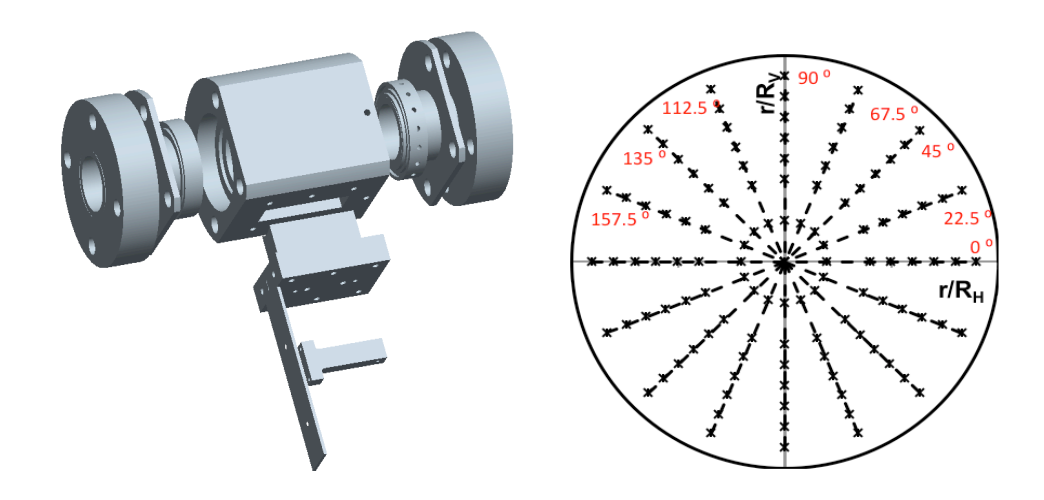


Figure 5 a) instrumentation port used in horizontal section b) Measurement scheme to obtain local two-phase flow parameters in the horizontal section.

Figure 6 shows the profiles of local void fraction and a_i measured across the pipe cross-section at port P4 for Run6 ($j_f = 3.0 \text{ m/s}$ and $j_{g,atm} = 0.35 \text{ m/s}$). Measurements along the azimuthal directions of 0° and 90° denote the horizontal and vertical axes of the pipe cross-section, respectively. It is interesting that most of the bubbles are distributed along the horizontal axis of the pipe cross-section and that the peak in the bubble distribution occurs approximately at a non-dimensional radius (r/R) of \pm 0.4. Since the measurements are obtained under bubbly flow conditions, the local a_i profiles are similar to the local void fraction profiles. The detailed measurements are used to generate three-dimensional profiles of local two-phase flow parameters. Figures 7a and 7b shows the three-dimensional profiles of measured local void fraction and a_i , respectively, at port P4. It is speculated that the bimodal bubble distribution along the horizontal axis of the pipe at port P4 is created by the secondary flow generated by the elbow as explained later.

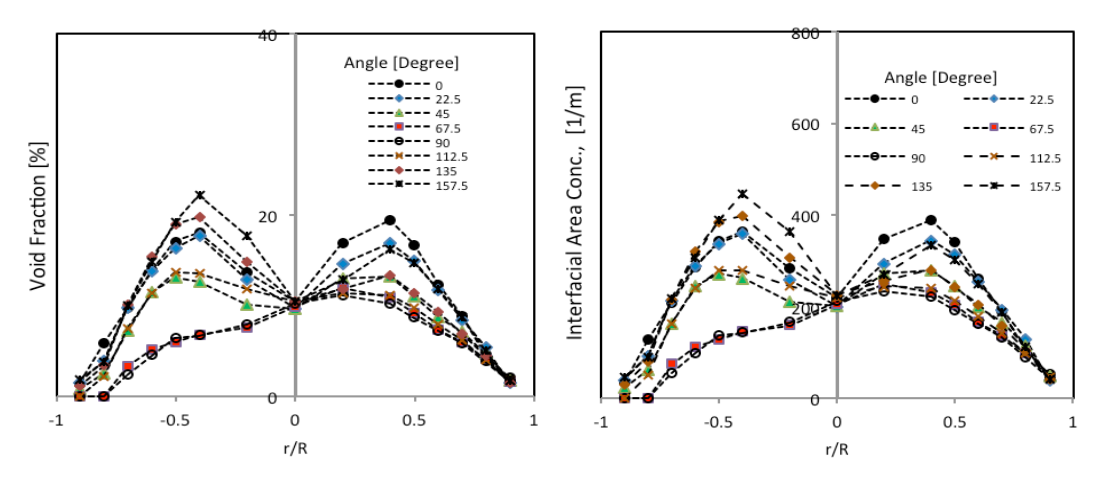


Figure 6 Local profiles of void fraction and interfacial area concentration for Run4 ($j_f = 3.0 \text{ m/s}$ and $j_{g,atm} = 0.14 \text{ m/s}$) measured at port P4 for different azimuthal angles.

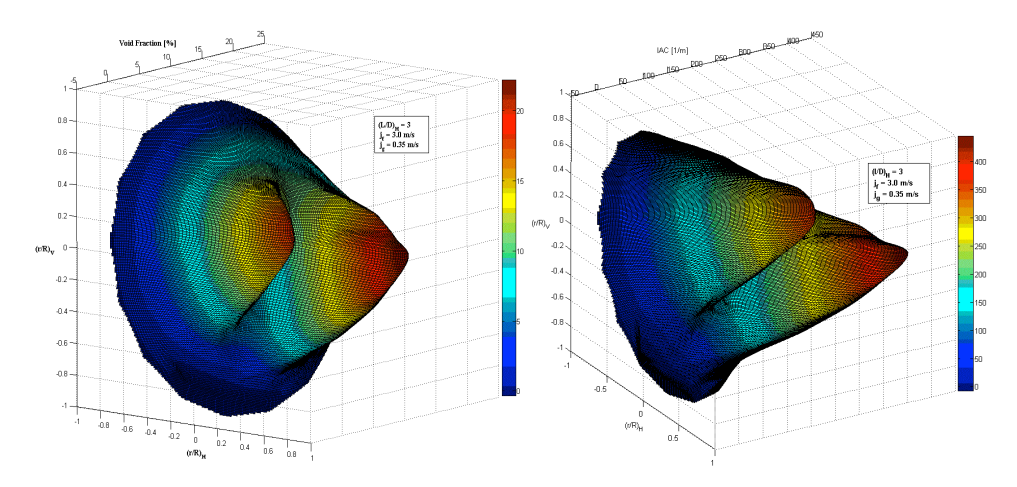


Figure 7 3-dimensional profiles of a) measured void fraction b) interfacial area concentration at port P4 for Run6 ($j_f = 3.0 \text{ m/s}$ and $j_{g,atm} = 0.35 \text{ m/s}$).

As fluid flows through elbows or pipe bends of any cross-section, the higher velocity fluid moving near the center of the pipe cross-section experiences a higher centrifugal force as compared to the slower moving fluid in the boundary layer. This causes the fluid at the center to move outward and the fluid flowing in the boundary layer to move inward, which creates a secondary flow in a plane perpendicular to the axial flow [8]. Ito [9] presents a comprehensive review on flow through various bends with different cross-sections under various flow conditions. However, there is a lack of experiments and knowledge on the effects of secondary flow on two-phase flow structure. In the present study, the experiments are performed within the bubbly flow regime, and the average bubble Sauter mean diameter at port P4 for all flow conditions is approximately 3-4 mm. It is speculated that the bubbles entering the elbow are entrained along the secondary flow streamlines and hence are distributed into two radial regions along the horizontal axis of the elbow cross-section in the plane perpendicular to the central axis of the elbow.

Further downstream at port P5, 30D from the vertical-upward elbow, the secondary flow effect on the bubble distribution decays, and buoyancy becomes the dominant force, pushing the

bubbles to the top of the pipe cross-section. Figure 8 shows the three-dimensional profile and contour plot of the local void fraction measured at port P5 for Run 6.

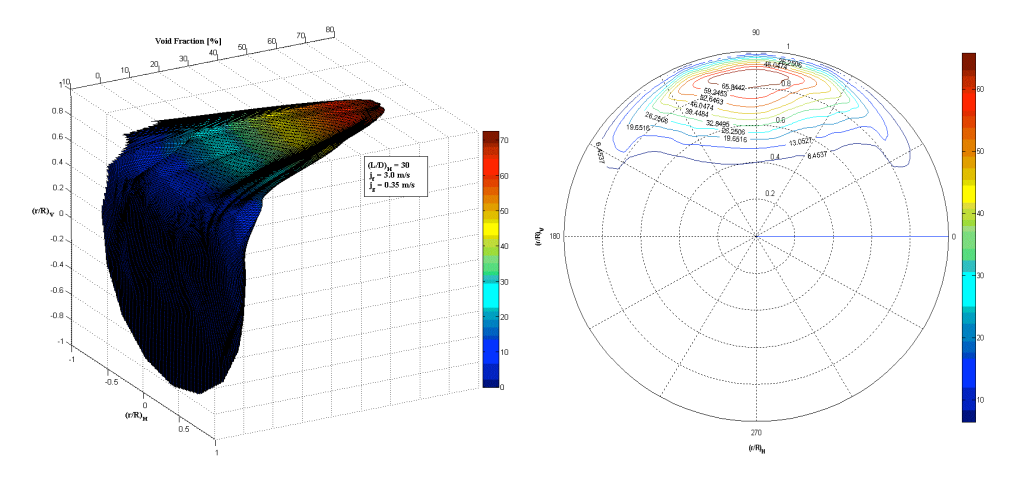


Figure 8 3-dimensional profiles and contour plots of measured void fraction at port P5 (33D downstream of the vertical elbow) for Run6 ($j_f = 3.0 \text{ m/s}$ and $j_{g,atm} = 0.35 \text{ m/s}$).

2.3 Interfacial structures in the vertical-downward section

In the vertical downward section, the local two-phase flow parameters are measured at ports P11, P12, and P14, which are located at 2.5D, 16.5D, and 66.5D downstream of the vertical-downward elbow. In order to capture the elbow effect, local data is acquired in four different radial directions by rotating the measurement port. For each radial direction 15 local measurements are made along the pipe diameter, leading to 60 data points across the cross-section. Figure 9 shows the coordinate system used in the vertical-downward section. The direction of flow is into the page, and r/R_C and r/R_P denote the non-dimensional radial axes along the curvature of the elbow and perpendicular to the curvature of the elbow, respectively. The radius towards the outside of the elbow's curvature and the fluid flow direction are taken as positive. Figure 10 shows the three-dimensional profiles of measured local void fraction and interfacial area concentration. As is evident from the figures, the local profiles peak towards the inside of the elbow curvature, which suggests that the bubbles migrate into this region. Although, the secondary flow circulation is expected, the flow is dominated by the inertial forces. Hence, the higher inertia liquid falls along the outer curvature of the elbow and forces the gas towards the inner curvature of the elbow.

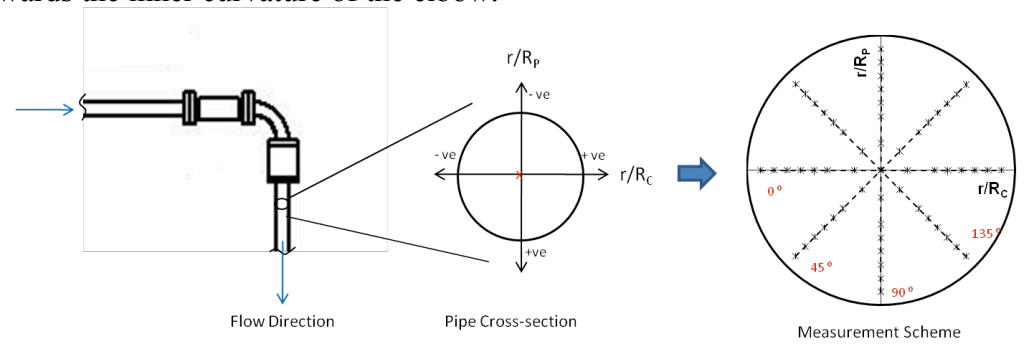


Figure 9 The coordinate system and measurement mesh for vertical-downward two-phase flow.

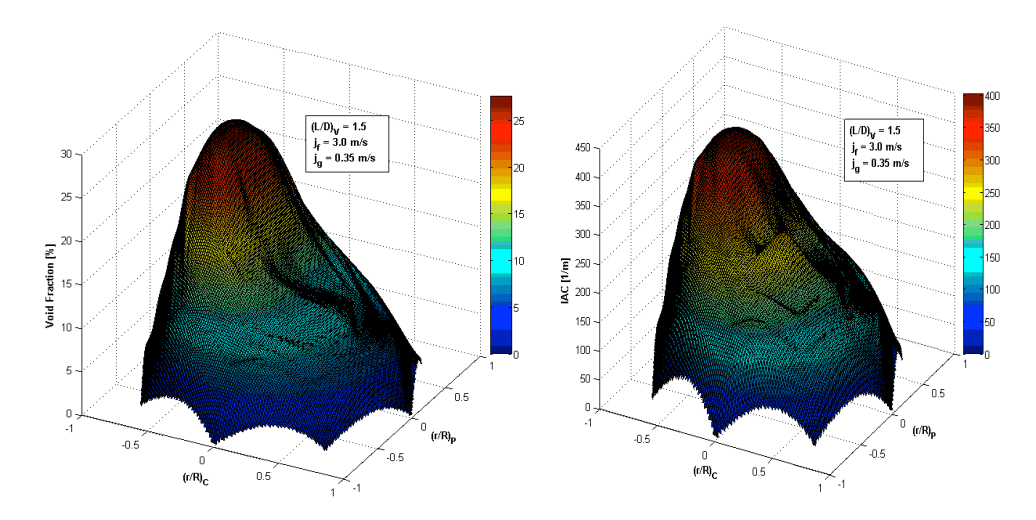


Figure 10 3-dimensional profiles of measured void fraction and interfacial area concentration at port P11, for Run6 ($j_f = 3.0 \text{ m/s}$ and $j_{g,atm} = 0.35 \text{ m/s}$).

It is observed that the elbow effect decays by port P12 and that the bubble distribution becomes symmetric across the flow axis. Figure 11 shows the local profiles of void fraction and a_i at ports P12 and P14. Further downstream at port P14 the bubbles start to accumulate in the center of the pipe causing a steep center-peak in the local void fraction profile. This suggests coring of the bubbles in the center of the pipe which is typical of the developed vertical downward two-phase bubbly flow.

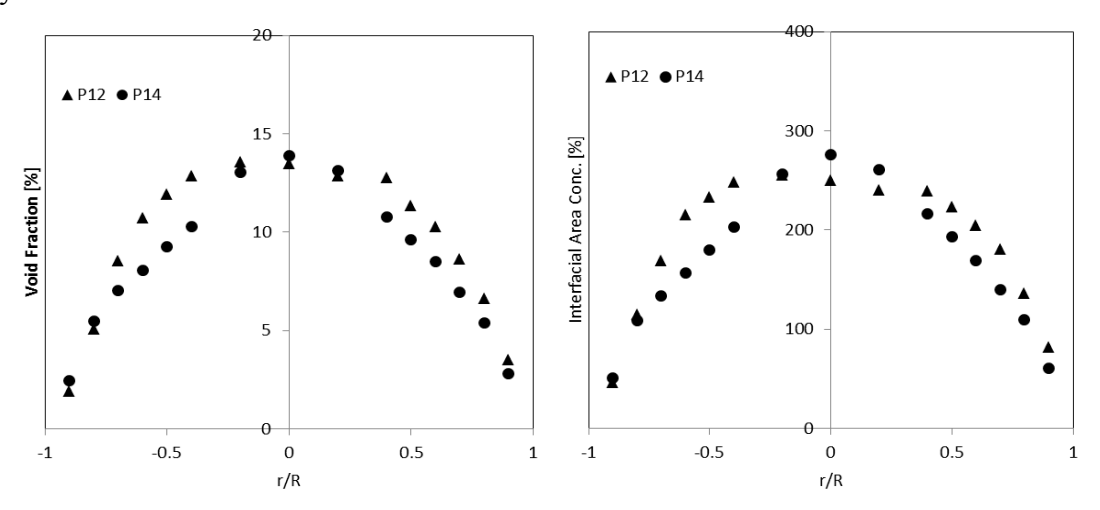


Figure 11 Local profiles of void fraction and interfacial area concentration at port P12 and P14 for Run6 ($j_f = 3.0 \text{ m/s}$ and $j_{g,atm} = 0.35 \text{ m/s}$).

The comprehensive development of the profiles of local void fraction along the combinatorial channel is shown in Figure 12. The figure shows the evolution of bubbly two-phase flow during different stages of development across the 90-degree vertical elbows. It is interesting that the elbows not only promote bubble interaction but also have a significant effect on the bubble distribution, which can provide insights into the flow regime transitions.

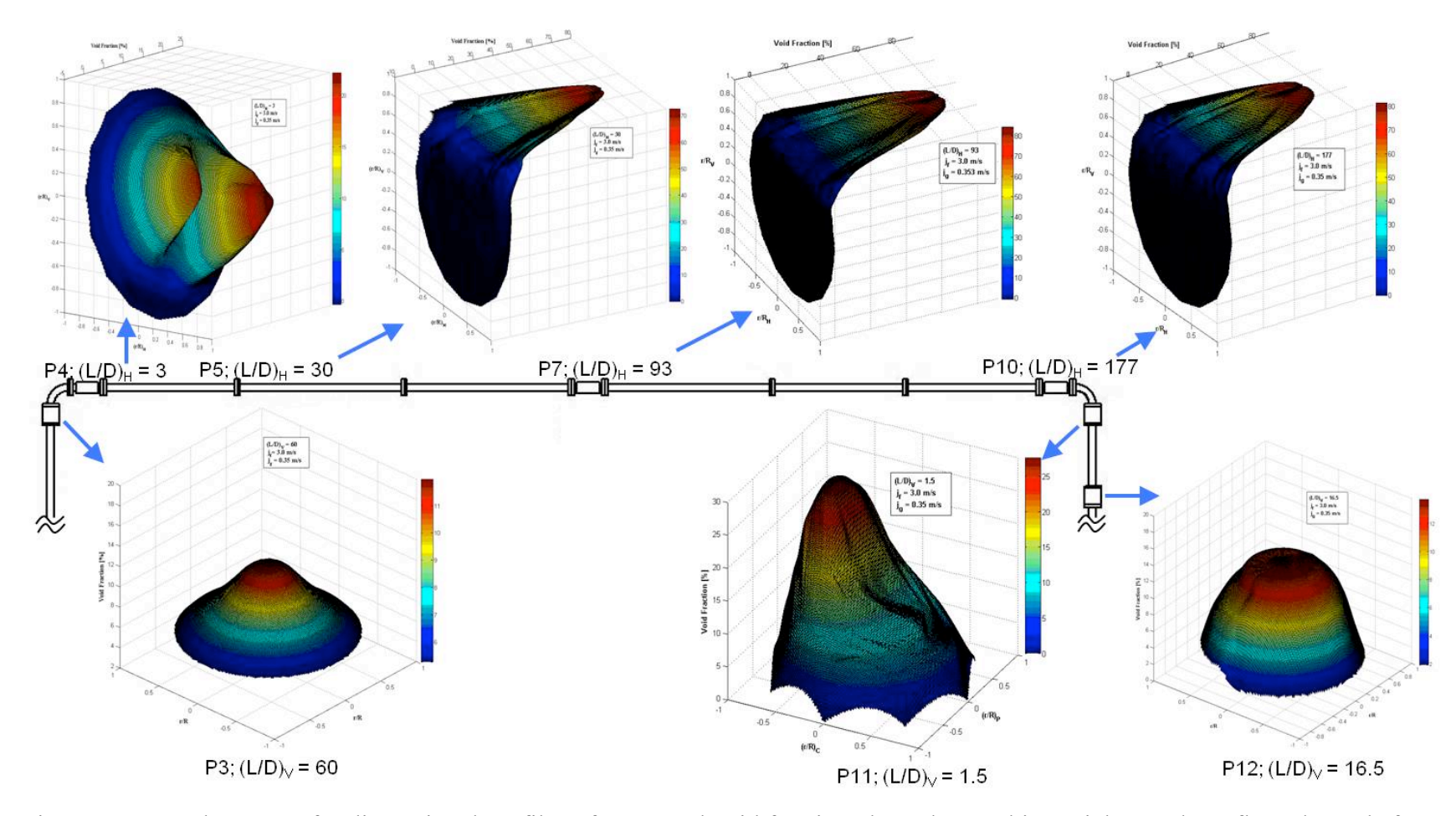


Figure 12 Development of 3-dimensional profiles of measured void fraction along the combinatorial two-phase flow channels for Run6 ($j_f = 3.0 \text{ m/s}$ and $j_{g,atm} = 0.35 \text{ m/s}$).

2.4 One-dimensional transport of interfacial structures

Figure 13 shows the transport of area-averaged void fraction, $\langle \alpha \rangle$, and area-averaged interfacial area concentration, $\langle a_i \rangle$, for constant liquid flow rate, j_f of 2.0 m/s, and increasing gas flow rates. The vertical lines represent the locations of the elbows and distinguish between the regions of vertical-upward, horizontal, and vertical-downward two-phase flow in the axial flow direction. It is observed that $\langle \alpha \rangle$ increases along the vertical-upward section which is attributed to the pressure drop along the vertical section which causes the bubbles to expand. Moving further downstream, it is observed that the $\langle \alpha \rangle$ decreases across the vertical-upward elbow and continues to gradually decrease along the horizontal section. The decrease in $\langle \alpha \rangle$ can be attributed to the acceleration of the bubbles across the elbow. Further downstream of the elbow, the change in $\langle \alpha \rangle$ along the horizontal section is mainly due to the frictional pressure drop. As the flow moves from the horizontal section to the vertical-downward section, a sharp rise in $\langle \alpha \rangle$ is observed across the vertical-downward elbow. Conventional analysis would attribute this to either a large pressure drop across the vertical-downward elbow or a large deceleration across the elbow. However, the pressure drop data reveals that there is a net increase in the static pressure across the elbow and the transport of void-weighted bubble velocity shows that there is an acceleration of the gas-phase across the elbow. Flow visualization across the elbow shows that there are regions of recirculation at port P11 and that large bubbles moving across the elbow tend to stay at the measurement location for an extended period of time before becoming entrained by the liquid. The higher residence time of the large bubbles and the recirculation causes the sharp increase in $<\alpha>$. Further downstream in the vertical downward section $<\alpha>$ decreases along the axial direction because the increase in pressure causes the bubbles to contract.

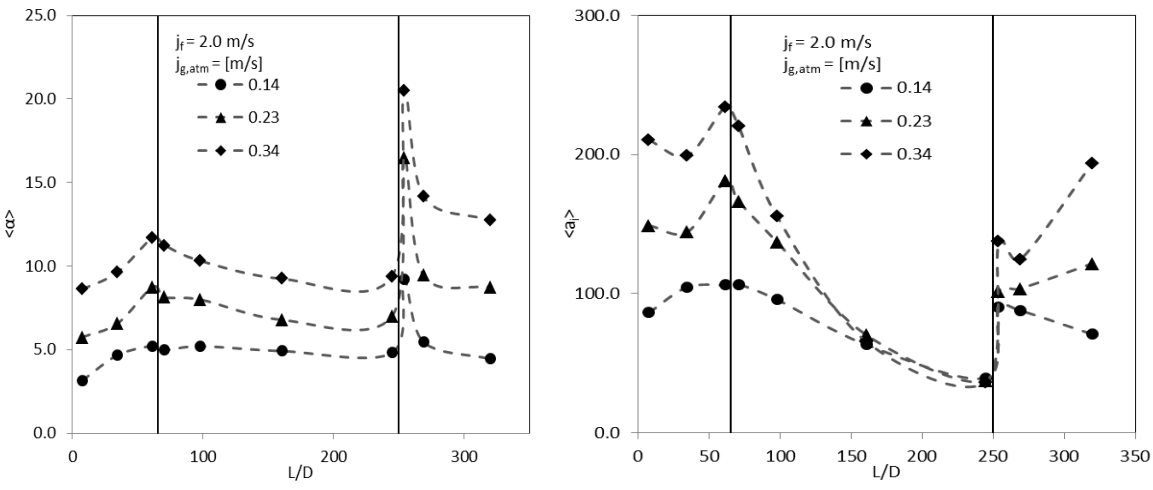


Figure 13 Axial development of $< \alpha >$ and $< a_i >$ for a constant liquid flow rate, $j_f = 2.0$ m/s, and increasing gas flow rates.

The transport of $\langle a_i \rangle$ in the vertical-upward section shows that with an exception of Run 1, $\langle a_i \rangle$ decreases between ports P1 and P2 and then increases between ports P2 and P3. Since, the two-phase flow is still developing at port P1, the decrease of $\langle a_i \rangle$ can be attributed to the inlet effect. Between ports P2 and P3 and across the vertical-upward elbow, the transport of $\langle a_i \rangle$ is similar to transport of $\langle a_i \rangle$, which is characteristic of the bubbly flow. However, there is a sharp decline in $\langle a_i \rangle$ for all flow conditions along the horizontal section. As the bubbles move along the horizontal section, they migrate towards the top of the pipe and coalesce to form larger plug or

slug bubbles. Hence, coalescence of the bubbles along the horizontal section causes a decrease in $\langle a_i \rangle$. An explanation similar to the transport of $\langle \alpha \rangle$ across the vertical-downward elbow follows for the transport of $\langle a_i \rangle$ across the vertical-downward elbow. Further downstream in the vertical-downward section, $\langle a_i \rangle$ either decreases or increases depending on the gas flow rate. At the lowest gas flow rate, $\langle a_i \rangle$ has a similar profile as that of $\langle \alpha \rangle$, which is characteristic of bubbly flows. However, for the higher gas flow rates the flow is characterized by presence of larger bubbles. Hence, an increase in $\langle a_i \rangle$ along the axial direction suggests breakup of the large bubbles.

The one-dimensional transport of $<\alpha>$ and $<a_i>$ for flow conditions with constant liquid flow rate of 3.0 m/s and increasing gas flow rate are shown in Figure 14. It is observed that $\langle \alpha \rangle$ increases along the axial direction in both vertical-upward and horizontal section. This can be attributed to the pressure drop along the axial direction which is due to hydrostatic head loss in the vertical upward section, minor losses across the vertical elbow, and frictional pressure loss along the length of the test section. Comparing the one-dimensional transport of <a;> along the vertical upward section, it is observed that for the flow condition with the lowest gas flow rate, ig atm of 0.14 m/s, $\langle a_i \rangle$ follows same trend as that of $\langle \alpha \rangle$, which is consistent with the behavior in the bubbly flow regime. However, at the flow conditions with higher gas flow rates, <a;> decreases between ports P2 and P3 in the vertical section, while $<\alpha>$ increases. This indicates that bubbles coalesce between ports P2 and P3 leading to a decrease in the interfacial area. Moreover, there is a sharp increase in $\langle a_i \rangle$ across the vertical elbow while $\langle \alpha \rangle$ increases gradually. This can be attributed to the disintegration of the bubbles caused by the elbow. There is a gradual increase in $<\alpha>$ along the horizontal section, while there is a small decrease in $<a_i>$. This is caused by coalescence of the bubbles along the horizontal section. Again, the transport of both $\langle \alpha \rangle$ and <a>i> across the vertical downward elbow shows a sharp increase which is attributed to recirculation and higher residence time of the bubbles at port P11. Further downstream of the vertical downward elbow, both $\langle \alpha \rangle$ and $\langle a_i \rangle$ decrease along the axial direction due to an increase in the local static pressure causing the bubbles to contract.

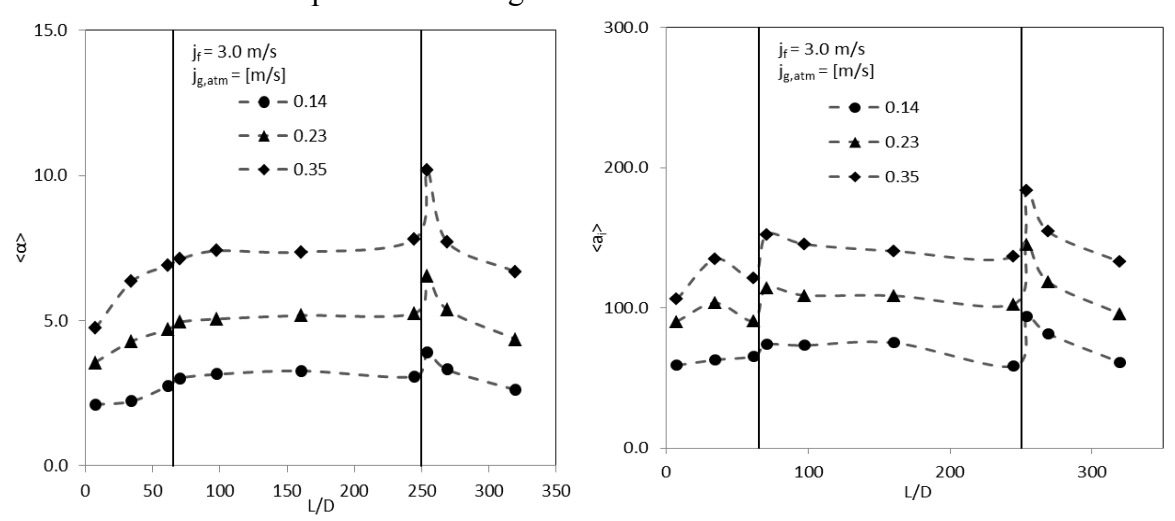


Figure 14 Axial development of $< \alpha >$ and $< a_i >$ for a constant liquid flow rate, $j_f = 3.0$ m/s, and increasing gas flow rates.

2.5 Interfacial area transport model predictions

This section presents preliminary results obtained using group-one interfacial area transport equation (IATE) for vertical-upward and vertical-downward section. The experimental values for void fraction, bubble velocity, interfacial area concentration and pressure at ports P1 and P11 are specified as boundary conditions for the vertical-upward and vertical-downward section, respectively. The empirical coefficients for the different bubble-interaction mechanisms are obtained from Wu et. al. [10] and Kim [11] for vertical-upward two-phase flow and Ishii et. al. [12] for vertical-downward two-phase flow.

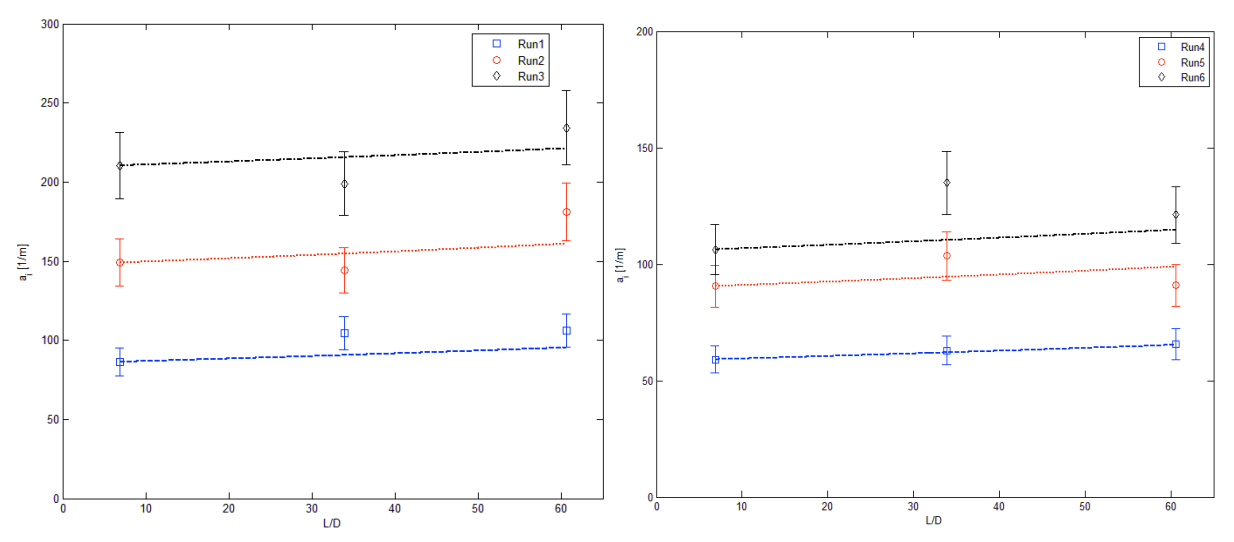


Figure 15 Comparison of model and experiment for a) Runs 1, 2 and 3 and b) Runs 4, 5 and 6 in vertical-upward section.

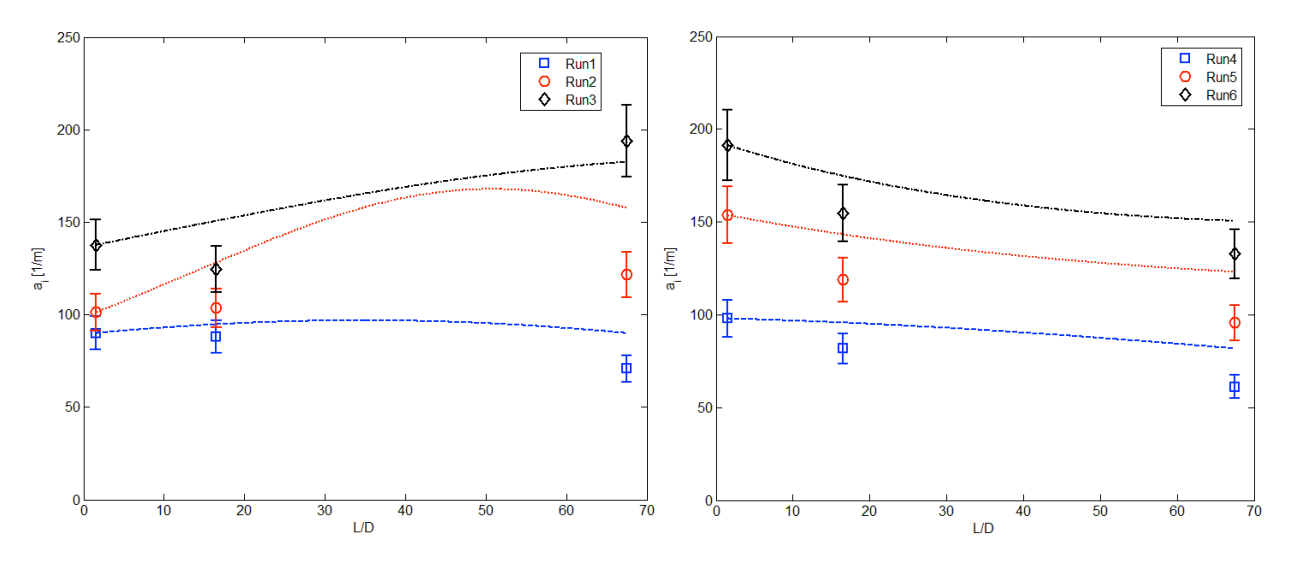


Figure 16 Comparison of model and experiment for a) Runs 1, 2 and 3 and b) Runs 4, 5 and 6 in vertical-downward section.

The comparison of the development of area-averaged interfacial area concentration with the model prediction in vertical-upward and vertical-downward two-phase sections is shown in Figures 15 and 16. The error bars shown are $\pm 10\%$ of the measured value. As mentioned earlier all of the flow conditions in the vertical-upward section are within the bubbly flow regime.

Hence, the group-one interfacial area transport model is used to predict the development of interfacial area concentration. The model prediction shows reasonably good agreement with the experimental data for all of the flow conditions in the vertical-upward section. However, in the vertical-downward section, Runs 1, 2, and 3, which corresponds to flow conditions with a constant liquid flow rate of 2.0 m/s and increasing gas flow rates, have a higher disagreement between the model predictions and the experiments. As observed in the previous sections, for Runs 1, 2 and 3, significant coalescence occurs in horizontal section. As such the inlet condition for the vertical-downward section consists of predominantly group-two bubbles. Since, the group-one IATE model is used, the presence of group-two bubbles leads to deviation in the predictions. Moreover, recirculation is observed for all the flow conditions at port P11. It is speculated that the disagreement between the model and the experimental data can also arise from the conductivity probe measurements under such flow conditions at port P11.

3. Conclusion

A four-sensor conductivity probe is used to obtain local two-phase flow parameters along a combinatorial channel. The effect of the elbow is demonstrated by a bimodal bubble distribution at the measurement location immediately downstream of the vertical-upward elbow. It is speculated that the bubbles are entrained into the two counter-rotating vortices generated by secondary flow in the vertical-upward elbow, leading to a dual-peaked profiles of local void fraction and a_i . Furthermore, it is found that the elbow effect on the bubble distribution decays by 30D downstream of the elbow, and the bubbles migrate to the top wall of the pipe cross-section due to buoyancy.

The axial transport of area-averaged void fraction and interfacial area concentration across the elbows show that the elbows promote bubble disintegration. For the 90-degree vertical upward elbow, it is found that while the bubbles accelerate across the elbow for flow conditions with a liquid flow rate of $2.0\,$ m/s, they decelerate across the elbow for flow conditions with a liquid flow rate of $3.0\,$ m/s. Preliminary one-group IATE model predictions are presented for vertical-upward and vertical-downward two-phase flow. It is found that the model predictions are in good agreement with the experimental measurements in the vertical-upward section within $\pm 10\%$. However, the disagreement between model predictions and measurements is found to be higher for vertical-downward two-phase flow. It is worth noting that the disagreement in the vertical-downward section arises from a combination of factors such as the presence of group-two bubbles and error in the probe measurements due to recirculation at port P11.

Acknowledgement

This research is supported by the U.S DOE through DOE NEER Program.

4. References

- [1] S. Kim, J. H. Park, G. Kojasoy and J. Kelly, "Interfacial structures in horizontal bubbly flow with 90-degree bend", Nuclear Engineering Design, Vol. 237, 2007, pp. 2105-2113.
- [2] J. Talley, S. Kim, T. Guo and G. Kojasoy, "Geometric effects of 45-degree elbow in horizontal air-water bubbly flow", Nuclear Technology, Vol. 167, No. 1, 2009, pp. 2-12.

- [3] M. Yadav, J. Talley and S. Kim, "Influence of horizontal return bend on the two-phase flow pattern in small diameter tubes", Journal of Fluids Engineering, Vol. 132, No. 11, 2010, pp. 145-152.
- [4] M. Yadav and S. Kim, "Experimental studies on air-water two-phase flow through a 90-degree vertical elbow", Proceedings of ANS ICAPP, 2010, San Diego, California, USA.
- [5] S. Kim, X. Y. Fu, X. Wang, and M. Ishii, "Development of the miniaturized four-sensor conductivity probe and the signal processing scheme", Int. J. Heat Mass Transfer, Vol. 43, 2000, pp. 4101-4118.
- [6] Q. Wu and M. Ishii, "Sensitivity study on double sensor conductivity probe for measurement of interfacial area concentration", Int. J. Multiphase Flow, Vol. 25, 1999, pp. 155-173.
- [7] Z. Rouhani, "Effect of wall friction and vortex generation on the radial distribution of different phases", Int. J. Multiphase Flow, Vol. 3, 1976, pp. 35-50.
- [8] H. Schlicting, "Boundary layer theory", McGraw-Hill, 1960, pp. 529-531.
- [9] H. Ito, "Flow in curved pipes", JSME International Journal, Vol. 30, 1987, pp. 543-552.
- [10] Q. Wu, S. Kim, M. Ishii, and S. G. Beus, "One-group interfacial area transport in vertical bubbly flow", Int. J. Heat Mass Transfer, Vol. 41, 1998, pp. 1103-1112.
- [11] S. Kim, "Interfacial area transport equation and measurement of local interfacial characteristics", PhD. Thesis, Purdue University, 1999.
- [12] M. Ishii, S. S. Paranjape, S. Kim, and X. Sun, "Interfacial structures and interfacial area transport in downward two-phase bubbly flow", Int. J. of Multiphase Flow, Vol. 30, No. 8, 2004, pp. 779-801.